Cyclic and creep combination effects on the long-term undrained behavior of overconsolidated clay

Jian HAN[1], Zhen-Yu YIN[2]✉, Christophe DANO[3] and Pierre-Yves HICHER[4]

[1] School of Materials Science and Mechanical Engineering, Beijing Technology and Business University, Beijing, 100048, China

[2] Department of Civil and Environmental Engineering, The Hong Kong Polytechnic University, Hung Hom, Kowloon, Hong Kong

[3] 3SR Laboratory, Grenoble Alpes University, UMR CNRS 5521, Grenoble, 38000, France

[4] Research Institute of Civil Engineering and Mechanics (GeM), Ecole Centrale de Nantes, UMR CNRS 6183, Nantes, 44300, France

✉ Correspondence to Dr. **Zhen-Yu YIN** (Phone: +852 34008470, Email: zhenyu.yin@polyu.edu.hk; zhenyu.yin@gmail.com)

Abstract: Soft soil subjected to cyclic loading typically exhibits an increase of excess pore pressure under undrained condition which brings the soil to an overconsolidated state. Then, under a subsequent large number of cycles (e.g. more than one million) which also takes time, the creep at overconsolidated state influences the cyclic effect and thus results in a complicated long-term undrained behavior. This paper aims to clarify this long-term undrained behavior of overconsolidated clay. The reconstituted samples are prepared from natural samples retrieved in the north of France. First, the shear strength characteristics along monotonic triaxial stress paths are identified. Then load control cyclic tests on overconsolidated specimens are conducted in fully saturated and undrained conditions. Small cyclic deviatoric stresses are applied in order to investigate more particularly the behavior under a very large number of cycles, during which an unusual pore pressure evolution is observed. To explain this, undrained triaxial creep tests are performed on reconstituted specimens with different values of OCRs under some specified stress states. The evolutions of axial strain, excess pore pressure, stress ratio, stress path, plastic strain rates and stress dilatancy during undrained creep are discussed. The additional undrained creep tests also show that two processes are simultaneously acting in a competitive manner: increase of the pore pressure due to the cyclic loading, decrease of the pore pressure because of creep.

Keywords: cyclic loading, creep; triaxial test; soft clay; constitutive relation; stress dilatancy

1. Introduction

Various design rules are proposed to geotechnical engineers to calculate both shaft capacity and base resistance of piles under axial or lateral loads. Most of these rules are calibrated from in situ tests (e.g., cone penetration test, pressuremeter test) that allow estimating the static capacity. However, there are more and more situations where geotechnical engineers may have to consider the effects of repeated loads with variable amplitude with time. Wind, waves, tides are examples of physical phenomena that induce cyclic loadings on structure foundations with very large number of cycles over the time. For soft clay, the cyclic behavior has been widely investigated during last decades (Andersen et al.[1]; Vucetic and Dobry [2]; Biarez and Hicher [3]; Hyodo et al. [4]; Li and Meissner [5]; Boulanger and Idriss [6]; Cai et al. [7]; Yin et al. [8]; Mortezaie and Vucetic [9]; Qian et al. [10,11]). However, long-term undrained cyclic behavior (e.g. more than one million) is still a critical issue which was not studied so much in the literature.

As well known, soft soil subjected to cyclic loading typically exhibits an increase of excess pore pressure under undrained condition which brings the soil to an overconsolidated state. Then, under a subsequent large number of cycles which also takes time, the creep at overconsolidated state generating negative excess pore pressure will definitely influence the cyclic behavior in long-term. Thus, the cyclic and creep coupling effect at overconsolidated state may result in a complicated long-term undrained behavior, which needs to be clarified.

Thus, to investigate this coupling behavior, the undrained creep behavior of overconsolidated clay may also be separately clarified. Up to now, the undrained creep behavior has been widely investigated for normally consolidated clay (e.g., Walker [12]; Arulanandan et al. [13]; Holzer et al. [14]; Vaid and Campanella [15]; Adachi and Oka [16]; Hinchberger [17], Yao et al. [18, 19]; Yin et al. [20]; Yin and Hicher [21]; Yin et al. [22, 23]; Wang and Yin [24]; Zhao et al. [25]). Overconsolidated clay was considered as relatively stiff foundation

soils and few studies on undrained creep (e.g., lightly overconsolidated clay by Tavenas et al. [26]) are available. However, besides of the above mentioned cyclic and creep coupling effect, the progressive failure of overconsolidated clay structures or foundations is also mainly due to the undrained creep under the undrained shear condition. Thus, the research in this respect cannot be ignored.

Therefore, this paper aims to clarify the long-term undrained behavior of overconsolidated clay to investigate both the response of soil specimens subjected to a very large number of cycles (about one million), and the undrained creep behavior of overconsolidated clay. Reconstituted samples are first prepared from natural samples. First, the shear strength characteristics along monotonic triaxial stress paths are identified. Then load control cyclic tests on overconsolidated specimens are conducted in fully saturated and undrained conditions. Small cyclic deviatoric stresses are applied in order to investigate more particularly the behavior under a very large number of cycles. Beside of this, undrained triaxial creep tests are performed on reconstituted specimens with different values of OCRs varying from 2 to 14 under the same stress path having the initial stress state for creeping lying almost on the critical state line in p'-q plane. Finally, the cyclic and creep processes simultaneously acting in a competitive manner are discussed: increase of the pore pressure due to the cyclic loading, and decrease of the pore pressure because of creep.

2. Tested clay

2.1 Description of clay and clay samples

The tested natural clay was sampled in the northern France (at Merville), at a depth between 5 and 11 meters. The plastic tube with a length of 1.0 m, inner diameter of 110 mm and a thickness of 1 mm was used for sampling. According to Josseaume et al. [27], the Merville clay was deposited during the Ypresian in a marine gulf stretching across the whole area which is now located in northern France, Belgium and southeastern

England. The soil surface stood probably about 200 m above the present surface of the clay at the Pliocene. The formations overlying the clay and the top of the clay layer were later eroded. This erosion process was sustained to Quaternary by the deposition of the Flandrian alluvial deposits. The clay layer has at the present time an effective vertical stress much lower than that existing during the Pliocene. Its origin is similar to the London clay, more studied in the literature. This highly plastic, stiff clay (w_L = 97 %, I_P = 59 %, OCR ≈ 30 in-situ) with dominant illite and smectite minerals exhibits a uniform appearance in the form of a grey brown material. However, because of their specific geological history, samples also have cementation and structuration in the form of pre-existing fissures, which prevent any comparative subsequent analysis.

To obtain more identical and homogeneous samples without influence of inter-particle bonds and occurrence of fissures, a mass of natural clay was first dried in an oven at 105°C, then ground to a powder state. The dry powder from natural samples was mixed with water at an initial water content equal to 1.5 times of the liquid limit (w_L) according to Burland [28] and then consolidated under one-dimensional condition for one month which is more or less one week longer than the duration of the primary consolidation based on Taylor's square root of time method. This ensures the full saturation and the complete consolidation. A vertical stress of σ'_{v0} = 100 kPa was applied for the consolidation.

2.2 Physical and mechanical properties

Some typical physical properties of the tested clay were measured and summarized in Table 1. Eight undrained triaxial tests in compression and two undrained triaxial tests in extension with isotropically consolidation and unloading stages were performed on the reconstituted specimens of Merville clay with different values of OCRs (here OCR = p'_{max}/p'_0, where p'_{max} is the maximum effective mean pressure during isotropic consolidation and p'_0 is the mean effective stress at the onset of shearing) varying from 1 to 14. The reconstituted specimens were

isotropically consolidated to a higher effective stress and maintained constant for one week, followed by an unloading stage to the target effective consolidation stresses for different tests. After the isotropic consolidation stage, the cell pressure was kept constant and the specimen was sheared to failure under undrained condition at a constant axial strain rate. The applied axial strain rate was 2.57 %/h for all undrained tests, with all results presented in Fig. 1. The slope of the critical state line (CSL) was obtained from stress paths in p'-q plane, based on which the slopes of CSL in compression (Mc = 1.0) and in extension (Me = 0.96) were measured. The compression and swelling indexes were obtained from e-log(p') curves. The assumed critical state line in the plane of e-log(p') is obtained with the same slope as the isotropic compression line in Fig. 2. The results of overconsolidated specimens did not reach the critical state line, since axial strains at the end of tests are not large enough for reaching the critical state. All these mechanical properties are also summarized in Table 1.

Note that the permeability of the reconstituted sample is about 3.2E-7 m/s, the generated pore pressure distribution inside of the specimen of Merville clay for such a high value of permeability should be homogenous during test according to Yin and Hicher (2008). To further confirm the uniformity of pore pressure, at the end of all the cyclic tests, water content from the top, the middle and the bottom part of each specimen has been measured and found identical. Besides, all the tests in this study are carried out in the constant temperature laboratory. The effect of the temperature is ignored. Thus, the measurement of pore pressure at the bottom of the specimen during the test should be reliable and representative.

3. Undrained cyclic tests

3.1 Test program and test procedure

All specimens for undrained triaxial cyclic tests are 35 mm in diameter and 70 mm in height. A device with the computer-controlled GDS dynamic triaxial testing system (10 HZ/1 kN) was used for all cyclic tests. After the

saturation stage verified by *B*-check (*B* value no less than 0.96 in this paper), all specimens were isotropically loaded up to a constant mean effective stress of 400 kPa with a back-pressure of 100 kPa within 3 days, and then consolidated at an isotropic effective stress of 400 kPa for another 7 days. After that, all specimens were unloaded isotropically to a mean effective stress of 100 kPa for obtaining an OCR of 4 within 2 days, and then stayed for another 2 days before undrained cyclic loading.

The undrained cyclic shearing was load-controlled. The mean deviatoric stress was null for all the tests. Therefore, the sine shape cycles are defined by the frequency set to 1 Hz and the cyclic stress half-amplitude q_{cyc}. Table 2 presents the initial characteristics of the four tested specimens. R_c is the ratio q_{cyc}/q_{max}, where q_{max} = 194.5 kPa is the undrained peak strength from a monotonic CIUC test on a specimen with OCR = 4. N_{cyc} is the total number of cycles attained for each test. Note that the frequency of 1 Hz was selected, which is different from the one of wind, waves or tides. In fact this is to ensure the test duration is reasonably not too short and not too long, e.g. for one million cycles requiring 12 days if 1 Hz is adopted. If the frequency is 10 Hz, the generated pore pressure inside of specimen may trend to inhomogeneous. If the frequency is 0.1 Hz, the duration is about 120 days for one million cycles which is a challenge for the apparatus and also faces many unexpected factors of laboratory like power cut-off.

3.2 General experimental results

All experimental results of four tests are presented in Fig. 3. Traditionally, the threshold stress ratio R_c can be found according to the simple method of Andersen [30, 31] with plotting synthetic diagrams using the data of cyclic shear stress, number of cycles, shear strains and so on. A high value of permenant shear train (e.g. 15%) is normally selected to estimate the threshold stress ratio R_c. However, based on Fig. 3 the strain levels of overconsolidated Merville clay after large number of cycles are still small, but some of stress paths in p'-q plane

have already reached the critical state line corresponding to which the clay can be considered in failure or not. For instance, at low stress ratio (i.e. R_c = 0.22), the cyclic effective stress paths did not reach the critical state lines, neither in compression nor in extension (Fig. 3(a)), and thus the clay is not in failure. For R_c = 0.44, the stress path exceeded the critical state line in extension only (Fig. 3(d)), and the clay is considered close to failure. For R_c = 0.48 and 0.52, the stress paths reached the two critical state lines in both compression and extension (Figs. 3(g), 3(j)), and the clay is considered in failure. A precise analysis of the experimental data for the tests CYC3 and CYC4 shows that the specimens failed before the end of the cyclic sequences: it was obvious for CYC4 in which the test was stopped after 6990 cycles. As observed during field tests on piles, it seems that the overconsolidated clay, even if the OCR values are different, exhibits a threshold value R_c of approximately 0.45 (a little bit bigger than 0.44 for which the clay is close to failure shown in Fig. 3(d)) below which cycles do not lessen significantly the soil resistance.

3.3 Evolution of axial strain

The axial strains versus number of cycles during cyclic loadings are presented in Fig. 4 for cyclic stress ratios from 0.22 to 0.52, in which the evolution of axial strain expands more significantly for higher cyclic stress ratio in general. Furthermore, permanent (mean) axial strain ($\varepsilon_a^{per} = (\varepsilon_a^{max}+\varepsilon_a^{min})/2$) and cyclic axial strain ($\varepsilon_a^{cyc} = (\varepsilon_a^{max}-\varepsilon_a^{min})/2$) are plotted with the number of cycles, shown in Fig. 5.

For comparison shown in Fig. 5(b), the test results on reconstituted Merville clay (main mineral: illite, $PI \approx$ 58.6 %, clay fraction CF = 26%, OCR = 4) were compared with data obtained by Andersen et al. [1] on Drammen clay (hydromica and feldspar, PI = 27 %, $CF \approx$ 50%, OCR = 4) and by Hicher [29] on both Black clay (kaolinite and illite, PI = 30 %, CF = 54 %, OCR = 4) and Bentonite clay (smectite, PI = 54 %, CF = 69 %, OCR = 4). As shown in Fig. 5(b), the sensibility of clay specimens to cyclic loading, through the evolution of

the cyclic axial strains, depends on the mineralogy related to the plasticity indexes *PI*. Clays (Drammen, Black clays) with smaller *PI* are thus more sensitive than clays with higher *PI* (Bentonite, Merville clay) because they present a weakest resistance to the evolution of their microstructure.

3.4 Evolution of excess pore pressure

The excess pore pressures versus number of cycles during cyclic loadings are presented in Fig. 6 for cyclic stress ratios from 0.22 to 0.52, in which the evolution of excess pore pressure expands with more significant amplitude for higher cyclic stress ratio in general. Furthermore, the evolutions of permanent (mean) pore pressure ($\Delta u^{per} = (\Delta u^{max}+\Delta u^{min})/2$) and cyclic pore pressure ($\Delta u^{per} = (\Delta u^{max}-\Delta u^{min})/2$) were plotted against the number of cycles in Fig. 7. Except for Test CYC4 with Rc = 0.52, the excess pore pressure started to increase as usually observed in cyclic tests but decreased until the end of the loading at large number of cycles. For this unusual phenomenon, the test procedure and equipment was carefully re-checked, e.g. consolidation was fully achieved before shearing and that no unexpected water leakage occurred.

Since the duration of the cyclic tests, with more than one million cycles, is about 12 days, the question of creep might be addressed. For this, the investigation of undrained triaxial creep behavior of overconsolidated clay was followed.

4. Undrained triaxial creep tests

4.1 Test program and test procedure

Reconstituted specimens for undrained creep tests series followed the same preparation procedure than previously described in section 3.1. All specimens were isotropically loaded up to a constant mean effective stress of 700 kPa with a back-pressure of 100 kPa within 3 days, and then consolidated for another 7 days. After

that, all specimens were unloaded isotropically to different mean effective stresses (=50 kPa, 100 kPa, 200 kPa and 350 kPa, respectively) for obtaining different values of OCR (=14, 7, 3.5 and 2, respectively) within 2 or 4 days, and then stayed for 2 days before undrained creep.

Four undrained creep tests were first performed under four deviatoric stress levels (Tests referred to be CRE1/OCR=2 to CRE4 / OCR=14 in Table 3), so that the initial stress state for creep converged quickly towards the critical state line in p'-q plane. The loading rate for the deviatoric stress for all tests was 50 kPa/min. For all creep tests, the vertical loadings were applied up to their target deviatoric stresses keeping the confining stress constant, which is a conventional way adopted by many researchers. To make sure whether the evolution of excess pore pressure is positive or negative for the test on the specimen with OCR=2, an additional test (named CRE5/OCR=2*) was performed by vertical loading applied simultaneously with confining stress unloading and keeping the constant mean effective stress. The creep test program is listed in Table 3. The slight difference between target values of stresses and real measured values (# symbol) is due to the stress control system of the triaxial equipment.

The criterion of creep test duration in this study is the axial strain rate decreasing at about 1E-7 /min, which is relatively small, so that the axial strain can be considered as stable, as for the tests with OCR=3.5, 7 and 14. For the case of axial strain rate increasing (tests at OCR=2), the test was stopped when the specimen failed.

4.2 Evolutions of axial strain and excess pore pressure

As mentioned above, the loading rate of deviatoric stress for all tests was 50 kPa/min. Thus, the vertical loadings of all creep tests reaching their target deviatoric stresses needed several minutes, i.e. the CRE1/OCR=2 needed 7 minutes to attain the target deviatoric stress. Most of the test results presented in the following figures include both loading stage and creep stage. However, in some cases, only the creep stage is presented, and the

time on the x-axis is therefore marked as “elapsed time of creep” in the figure, i.e. Figs. 9 and 12.

Regarding to the first four conventional creep tests as shown in Fig. 8(a), the axial compressive strain increases generally with time for each test, which is similar to the same type of test on normally consolidated and slightly overconsolidated clays. Beside of this, higher OCR involves smaller strain levels which is consistent with the phenomena observed during conventional shear tests (Fig. 1(d)), i.e. higher OCR results in higher stiffness of “q/p’-ε_a”. The test “CRE1/OCR=2” goes to failure in a few hours due to a high deviatoric stress level on a slightly overconsolidated clay specimen. The test “CRE5/OCR=2*” goes faster to failure than the test “CRE1/OCR=2” due to its higher initial stress ratio for creeping. The filled symbols presented in Fig. 8 represent the end of loading stage, in other word, the creep stage starts.

For the time evolution of excess pore pressure as shown in Fig. 8(b) during creep stage, the more heavily overconsolidated clays (OCR=3.5, 7 and 14) exhibit first a quick increase with an amount almost equal to one-third of the applied deviatoric stress at which point the stress ratios (q/p') are on the critical state line in p’-q plane, and then a long duration of decrease up to negative values (namely dilation). Higher OCR results in more negative excess pore pressure or dilation. For the lightly overconsolidated clay (OCR=2), the excess pore pressure of the test “CRE1/OCR=2” develops quickly resulting in the stress state on the critical state line. The excess pore pressure of the test “CRE5/OCR=2*” changes slightly because of stress control system during the loading and remains constant with the stress state on the critical state line. To distinguish the initial minutes on the curves of the results presented in Figs. 8(a) and (b), these curves are enlarged in Figs. 8(c) and (d), respectively.

4.3 Evolutions of stress ratio and stress path

The relationship between the stress ratio q/p' and the elapsed time of creep is presented in Fig. 9. At the

beginning of the creep stage for all the overconsolidated clays, the stress ratios reach the critical state line (q/p'=1.0) immediately and even are slightly beyond the critical state line. Then there is a long duration of decrease below the critical state line for heavily overconsolidated clays (OCR=3.5, 7 and 14). Except for the test "CRE5/OCR=2*", the elapsed time of creep for reaching the critical state line will be longer for the lower OCR. As mentioned above, the overconsolidated clay with higher OCR has higher stiffness. Thus, the stress ratio of the overconsolidated clay with the higher stiffness (due to higher mean effective stress) reaches the critical state line faster during creep.

To understand the evolution of stress ratio clearly, we divided creep tests into two processes. One is from the beginning of loading to the maximum value of stress ratio (Fig. 10(a)), which may include the creep stage for some tests, the other from the maximum value of stress ratio to the end of creep test (Fig 10(b)). In Fig. 10, each value of time shown above the critical state line represents the elapsed time of creep when the stress ratio reaches the maximum value for each creep test. For example, the value of time "300th min" represents the elapsed time of creep when the stress ratio reaches the maximum value for the test "CRE1/OCR=2". And values of time shown below the critical state line, three values (100th min, 10th min and 1st min) in Fig. 10(a) and four (100th min, 1000th min, 10000th min and end of creep) in Fig. 10(b), represent the elapsed time of creep for the thick dot-dash lines (for tests CRE1/OCR=2 to CRE4/OCR=14). The solid point for each test result shown in Fig. 10(a) represents the end of vertical loading, that means the creep beginning at constant vertical pressure.

At the end of vertical loading, the stress state for test “CRE5/OCR=2*” nearly reaches the critical state, and in few minutes, the specimen is broken as shown in Fig. 10(a). The three time lines (1 min, 10 min and 100 min) are more and more close to the critical state line as the creep time increases. These lines all intersect with the critical state line. As the value of OCR increases, the tangent point moves down along the critical state line. That

means creep test with higher OCR can reach the same target stress ratio (q/p'=1.0) faster. Whereas, in Fig. 10(b), the time lines (100^{th} min, 1000^{th} min and 10000^{th} min) are far away from the critical state line as the creep time increases. The points representing the end of creep tests, corresponding to the axial strain rate decreasing at 10^{-7} /min, are also shown in Fig. 10(b). A unique curve is obtained based on these points.

Likewise, we divided creep tests into two processes in e-log(p') plane, except for the test "CRE5/OCR=2*". One is from the beginning of loading to the maximum value of stress ratio (Figs. 11(a), 11(b) and 11(c)), the other from the maximum value of stress ratio to the end of creep test (Fig. 11(d)). In Fig. 11(a), the stress state of the test "CRE1/OCR=2" nearly reaches the critical state immediately after the creep stage beginning, conversely, the points representing the results on highly overconsolidated clays (OCR=3.5, 7 and 14) have some distance to the critical state line. As the creep time increases, all the thick dot-dash lines (representing the position after a same test duration) are far away from the critical state line (Figs. 11(a), 11(b) and 11(c)). That indicates that values of effective mean stresses decrease with the creep time increase, until the value of stress ratio (q/p') becomes maximum. As mentioned above, when the maximum stress ratio is reached, the stress paths reach the critical state line in p'-q plane, except the result of the test "CRE5/OCR=2*". That implies that though the stress ratio of overconsolidated clay reaches the critical state line, the specimen does not reach the critical state.

Inversely, in Fig. 11(d), the time lines (100^{th} min, 1000^{th} min and 10000^{th} min) are more and more close to the critical state line as the creep time increases. The points representing the end of creep tests, corresponding to the axial strain rate decreasing at about 1E-7 /min, are also shown in Fig. 11(d). A unique curve is obtained based on these points. This curve has some distance to the critical state line, indicating that highly overconsolidated clays (OCR=3.5, 7 and 14) do not reach the critical state. This phenomenon is consistent with the phenomena of the non monotonic evolution of excess pore pressure as well as the stable evolution of axial strain (Fig. 8(b)).

4.4 Evolutions of plastic strain rates

How to obtain the incremental plastic deviatoric strain and incremental plastic volumetric strain is presented in the Appendix of this paper. Thus, the evolution of plastic deviatoric strain rate with creep time is shown in Fig. 12(a) and the evolution of plastic volumetric strain rate versus creep time in Fig. 12(b).

At the beginning of the creep stage, the plastic deviatoric strain rate is very large for the test "OCR=2*", and the specimen fails in few minutes. For highly overconsolidated clays (OCR=3.5, 7 and 14), the plastic deviatoric strain rate decreases linearly in a log-log plot with the increase in time at the beginning of the creep stage. The slope of this relationship is independent of the creep stress. As the creep time increases (beyond 1E4 min), all three lines are shifted vertically downward, as indicated in Fig. 12(a). The onset of failure for the lightly overconsolidated clay (OCR=2) is signaled by the reversal in slope, as shown by the two topmost curves. As mentioned above, all the creep tests have the same target stress ratio and can reach the critical state line, but just specimens with lightly overconsolidation ratio (OCR=2) are broken during the creep. This phenomenon indicates that, at the same stress ratio, the applied vertical constant stress is the most important factor influencing the failure of specimens.

The more important OCR is, the more important the plastic volumetric strain rate at the beginning of the creep (Fig. 12(b)) is. Then, the strain rate decreases in a log-log plot with the increase in time, except for the constant strain rate of the test "CRE5/OCR=2*". The incremental plastic volumetric strain rate at the end of the test "OCR=2" is 3.2E-4 %/min, which indicates that the specimen is in the dilative state all the time during creep, although the volumetric strain during undrained creep test is equal to zero. This phenomenon of the reconstituted Merville clay in this paper has also been observed from the undrained creep tests on a soft clay – Wenzhou clay (Wang and Yin [24]). The plastic volumetric strain rates are -2.6E-5 %/min, -7.4E-5 %/min and

-8.6E-5 %/min at the end of creep stages for the specimens with OCR= 3.5, 7 and 14, respectively presented in Fig. 12(c). The filled symbols represent the end of creep stages. For highly overconsolidated clays, the specimens are firstly in the shear shrinkage state and then in the shear dilatancy state during creep.

4.5 Evolutions of stress dilatancy

Based on the plastic strain rates in the previous section, the evolution of dilatancy defined as $d = \mathrm{d}\varepsilon_{\mathrm{v}}^{\mathrm{p}} / \mathrm{d}\varepsilon_{d}^{\mathrm{p}}$ can be obtained. Similarly to the stress-dilatancy relationship, the $d = \mathrm{d}\varepsilon_{\mathrm{v}}^{\mathrm{p}} / \mathrm{d}\varepsilon_{d}^{\mathrm{p}}$ is plotted against the stress ratio starting from creep points in Fig. 13 for all five creep tests.

During the short duration after rapid loadings, all specimens start with positive values of d representing the contractive behavior and corresponding to the quick increase of excess pore pressure in Fig. 8(b). Then, d becomes zero whereas the stress ratio $q/p' = 1$ corresponding to the stress states lying on the critical state line in Fig. 10(a). The dilatancy d continuously decreases up to a minimum value representing a maximum dilation, and then increases towards zero with the stress ratio decreasing. The points representing the beginning of dilatancy increasing is marked by filled symbols with the creep time (Fig. 13). It is shown that higher OCR has a potential of smaller value of stress ratio for $d = 0$. The higher OCR specimens require more time for the dilatancy d reaching the minimum value shown in Fig.13.

4.6 Discussion of combined effects of cyclic loading and creep

Fig. 14 shows comparisons of excess pore pressures versus number of cycles or time between undrained triaxial cyclic tests under different cyclic stress ratios and undrained triaxial creep tests under different over-consolidation ratios. For the two creep tests with OCR=2, the creep tests attained tertiary creep, and the axial strains are both more than 20% as shown in Fig. 8 and Fig. 12, with increasing excess pore pressure. But

this is not the case to explain cyclic tests because cyclic tests are on much higher overconsolidated clay specimens. However, the creep tests at OCR=3.5, 7 and 14 with lower deviatoric stress levels are comparable to cyclic tests. These creep tests did not attain tertiary creep, and the specimens were not in rupture for long creep time. A significant decreasing of excess pore pressure for long creep time can be found in these tests. Thus, this phenomena can be reasonably considered for the compensation mechanism between pore pressure generation (cyclic) and reduction (creep) for the cyclic tests with large number of cycles.

It can be seen after certain moment (e.g. approximately 300 minutes from the figure) a continuous decrease of the pore pressure due to creep, which can also explain the specific evolution of the excess pore pressure during cyclic tests where cycles and creep can be considered as two opposed mechanisms over the test period. Since these additional creep tests showed that two processes were simultaneously acting in a competitive manner: increase of the pore pressure due to the cyclic loading, and decrease of the pore pressure because of creep, the two mechanisms "increase of the excess pore pressure due to cycles and simultaneous decrease due to creep" should be considered for the interpretation of results.

5. Conclusions

In order to clarify this long-term undrained behavior of overconsolidated clay with both cyclic effect and creep effect, the reconstituted samples are prepared from natural samples retrieved in the north of France. Before the investigation of long-term behavior, the shear strength characteristics along monotonic triaxial stress paths are identified on specimens with different ratios of over-consolidation and in both compression and extension conditions.

Then, load control cyclic tests on overconsolidated specimens are conducted in fully saturated and undrained conditions. Small cyclic deviatoric stresses are applied in order to investigate more particularly the behavior

under a very large number of cycles. It was shown that even after one million cycles, failure did not necessarily occur in most of the specimens unless the cyclic stress level was greater than a critical value. By comparison with previous data published in the literature, at similar over-consolidation ratio of 4, we show that mineralogy and plasticity indexes play a fundamental role on the resistance to cyclic loads. This also confirms the possible existence of a threshold stress ratio below which cycles have only a small effect on the soil resistance.

Moreover, during cyclic undrained triaxial tests, with an unusual number of cycles larger than one million, at a frequency of 1 Hz, an unusual pore pressure reduction is observed. This reveals that two mechanisms have to be considered: increase of the excess pore pressure due to the cycles and simultaneous decrease due to creep under highly overconsolidated state. To explain this, undrained triaxial creep tests are performed on reconstituted specimens with different values of OCRs under some specified stress states. The evolutions of axial strain, excess pore pressure, stress ratio, stress path, plastic strain rates and stress dilatancy during undrained creep are discussed: (1) Higher OCR has smaller creep strain level corresponding to higher stiffness. (2) The stress ratios reach and can be beyond the critical state line at the beginning of the creep stage, and the overconsolidated clay with higher stiffness reaches the critical state line faster during creep. (3) For highly overconsolidated clays (OCR=3.5, 7 and 14), the strain rate decreases linearly with increase of time in the log-log plane. The slope of this relationship is independent of the creep stress. The relationships are concave upward as shown with the failure for the lightly overconsolidated clays (OCR=2). This phenomenon indicates that, at the same stress ratio, the applied vertical constant stress is the most important factor influencing whether the specimens fail or not. (4) Though the incremental axial strain rate reaches the criteria of creep test duration, regarded as stable at the end of creep, the evolution of excess pore pressure non monotonically changes with the time increasing. That makes highly overconsolidated clays (OCR=3.5, 7 and 14) not reach the critical state. (5) Higher OCR has a potential of smaller value of stress ratio for d = 0. To reach the criteria of creep test duration takes much more time for

higher OCR.

The additional undrained creep tests also show that two processes are simultaneously acting in a competitive manner: increase of the pore pressure due to the cyclic loading and decrease of the pore pressure because of creep, which should be considered when interpreting results.

Further works will be carried out on performing a series of coupling cycle and creep tests by adjusting load frequency combined with Computed-Tomography investigation of internal microstructures of the samples, and modelling the combined effects of cyclic and creep for engineering practice.

Acknowledgements

This research was financially supported by the Research Grants Council (RGC) of Hong Kong Special Administrative Region Government (HKSARG) of China (Grant No.: 15217220, R5037-18F)

Reference

1. Andersen, K.H., Pool, J.H., Brown S.F., and Rosenbrand W.F. (1980) Cyclic and static laboratory tests on Drammen clay. Journal of the Geotechnical Engineering, 106 (GT5): 499–529

2. Vucetic, M., and Dobry, R. (1988) Degradation of marine clays under cyclic loading. Journal of Geotechnical Engineering, 114(2): 133–149

3. Biarez, J., and Hicher, P.Y. (1994) Elementary mechanics of soil behaviour: saturated remoulded soils. A.A.Balkema Publishers, Rotterdam

4. Hyodo, M., Yamamoto, Y., and Sugiyama, M. (1994) Undrained cyclic shear behaviour of normally consolidated clay subjected to initial static shear stress. Soils and Foundations, 34(4): 1–11

5. Li, T., and Meissner, H. (2002) Two-surface plasticity model for cyclic undrained behavior of clays. Journal of Geotechnical and Geoenvironmental Engineering, 128(7): 613–626

6. Boulanger, R.W., and Idriss, I.M. (2006) Liquefaction susceptibility criteria for silts and clays. Journal of Geotechnical and Geoenvironmental Engineering, 132(11): 1413–1426

7. Cai, Y., Gu. C., Wang. J., Juang, C., Xu, C.J., and Hu, X.Q. (2013) One-Way Cyclic Triaxial Behavior of Saturated Clay: Comparison between Constant and Variable Confining Pressure. Journal of Geotechnical and Geoenvironmental Engineering, 139(5): 797–809

8. Yin, Z.Y., Xu, Q., and Chang, C.S. (2013) Modeling cyclic behavior of clay by micromechanical approach. Journal of Engineering Mechanics, 139(9): 1305–1309

9. Mortezaie, A., and Vucetic, M. (2016) Threshold Shear Strains for Cyclic Degradation and Cyclic Pore Water Pressure Generation in Two Clays. Journal of Geotechnical and Geoenvironmental Engineering, 142(5): 04016007. doi:10.1061/(ASCE)GT.1943-5606.0001461.

10. Qian, J.G., Wang, Y.G., Yin, Z.Y., and Huang, M.S. (2016) Experimental identification of plastic shakedown behavior of saturated clay subjected to traffic loading with principal stress rotation. Engineering Geology, 214: 29–42

11. Qian, J.G., Du, Z.B., and Yin, Z.Y. (2018) Cyclic degradation and non-coaxiality of soft clay subjected to pure rotation of principal stress directions. Acta Geotechnica, 13(4): 943–959

12. Walker, L.K. (1969) Undrained creep in a sensitive clay. Géotechnique, 19(4): 515–529

13. Arulanandan, K., Shen, C.K., and Young, R.B. (1971) Undrained Creep Behavior of a Coastal Organic Silty Clay. Géotechnique, 21(4): 359–375

14. Holzer, T.L., Hoeg, K., and Arulanandan, K. (1973) Excess pore pressure during undrained clay creep. Canadian Geotechnical Journal, 10(12): 12–24

15. Vaid, Y.P., and Campanella, R.G. (1977) Time-dependent behaviour of undisturbed clay. Journal of Geotechnical Engineering, 103(7): 693–709.

16. Adachi, T., and Oka, F. (1982) Constitutive equations for normally consolidated clay based on elasto-viscousplasticity. Soils and Foundations, 22(4): 57–70

17. Hinchberger, S.D. (1996) The behaviour of reinforced and unreinforced embankments on rate sensitive clayey foundations. Thesis at University of Western Ontario, Canada

18. Yao, Y.P., Hou, W., and Zhou, A.N. (2009) UH model: three-dimensional unified hardening model for overconsolidated clays. Géotechnique, 59(5): 451–469

19. Yao, Y.P., Kong, L.M., Zhou, A.N., and Yin, J.H. (2015) Time-dependent unified hardening model: three-dimensional elastoviscoplastic constitutive model for clays. Journal of Engineering Mechanics, 141(6):1–18

20. Yin, J.H., Zhu, J.G., and Graham, J. (2002) A new elastic viscoplastic model for time-dependent behaviour of normally and overconsolidated clays: Theory and verification. Canadian Geotechnical Journal, 39(1): 157–173

21. Yin, Z.Y., and Hicher, P.Y. (2008) Identifying parameters controlling soil delayed behaviour from laboratory and in situ pressuremeter testing. International Journal of Numerical and Analytical Methods in Geomechanics, 32(12): 1515–1535

22. Yin, Z.Y., Chang, C.S., Karstunen, M., and Hicher, P.Y. (2010) An anisotropic elastic viscoplastic model for soft soils. International Journal of Solids and Structures, 47(5): 665–677

23. Yin, Z.Y., Yin, J.H., and Huang, H.W. (2014) Rate-dependent and long-term yield stress and strength of soft Wenzhou marine clay: experiments and modeling. Marine Georesources & Geotechnology, doi:10.1080/1064119X.2013.797060.

24. Wang, L.Z., and Yin, Z.Y. (2015) Stress-dilatancy of natural soft clay under undrained creep condition. International Journal of Geomechanical, 15(5):1–5.

25. Zhao, D., Hattab, M., Yin, Z.Y., and Hicher, P.Y. (2018) Dilative Behavior of Kaolinite under Drained Creep Condition. Acta Geotechnica, doi:10.1007/s11440-018-0686-x

26. Tavenas, F., Leroueil, S., La-Rochelle, P., and Roy, M. (1978) Creep behavior of an undisturbed lightly overconsolidated clay. Canadian Geotechnical Journal, 15(3): 402–423

27. Josseaume, H., Hieng, I. O., and Stempfelet, J. P. (1991). Détermination des paramètres de compressibilité d'une argile raide à partir d'essais oedométriques à haute pression. Bulletin de LCPC, 109-120 (in French).

28. Burland, J.B. (1990) On the compressibility and shear strength of natural soils. Géotechnique, 40(3): 329–378

29. Hicher, P.Y. (1979) Contribution à l'étude de la fatigue des argiles. PhD thesis, Ecole Centrale de Paris, France (in French)

30. Andersen, K.H. (1988). Properties of soft clay under static and cyclic loading. International Conference on Engineering Problems of Regional soils. Beijing, China. Proceeding: 7-26.

31. Andersen, K.H. (2004). Cyclic clay data for foundation design of structures subjected to wave loading. Proceedings of the International Conference on "Cyclic Behaviour of Soils and Liquefaction Phenomena", Bochum, Germany. : 371-387.

Appendix. Determination of plastic strain rates

The undrained triaxial condition implies null volumetric strain ($\mathrm{d}\varepsilon_\mathrm{a} + 2\mathrm{d}\varepsilon_\mathrm{r} = 0$). Thus, during undrained creep the incremental deviatoric strain can be obtained:

$$\mathrm{d}\varepsilon_\mathrm{d} = \frac{2}{3}(\mathrm{d}\varepsilon_\mathrm{a} - \mathrm{d}\varepsilon_\mathrm{r}) = \mathrm{d}\varepsilon_\mathrm{a} \tag{A1}$$

Because of the null change of the deviatoric stress during undrained creep test, the elastic deviatoric strain increment is null. Therefore, the Eq.(A1) can be used for the incremental plastic deviatoric strain.

The null volumetric strain condition also implies the relationship "$\mathrm{d}\varepsilon_\mathrm{v}^\mathrm{p} = -\mathrm{d}\varepsilon_\mathrm{v}^\mathrm{e}$" between plastic and elastic volumetric strains. Thus, the increment of plastic volumetric strain can be obtained by the change of mean effective stress due to the generation of excess pore pressure (dp'=-du), as follows:

$$\mathrm{d}\varepsilon_\mathrm{v}^\mathrm{p} = \frac{du}{K} \tag{A2}$$

with the bulk modulus $K = (1+e_0)\,p'/\kappa$ and $p' = p_0 + \Delta q/3 - \Delta u$.

Tables

Table 1. Physical and mechanical properties of Merville clay

Liquid limit (w_L)	97.2±1 %
Plastic limit (w_P)	38.6±1 %
Plasticity index (PI)	58.6±2 %
Specific gravity of solids (G_s)	2.65±0.2
Percent finer than 2 μm (CF)	26 %
Initial water content* (w_0)	50.1 %
Initial void ratio* (e_0)	1.28
Compression index* (C_c)	0.6
Swelling index* (C_s)	0.091
Slope of CSL in compression* (M_c)	1.0
Slope of CSL in extension* (M_e)	0.96

Remarks: * for reconstituted samples in this study.

Table 2. List of undrained triaxial cyclic tests on reconstituted specimens of Merville clay

Test	w (%) before cyclic	q_{cyc} (kPa)	R_c	OCR	N_{cyc}
CYC1	37.4	41.7	0.22	4	1,060,200
CYC2	37.0	84.7	0.44	4	1,051,480
CYC3	37.7	92.8	0.48	4	1,050,520
CYC4	38.5	101.0	0.52	4	6,990

Remarks: CYC representing cyclic test.

Table 3. List of undrained triaxial creep tests on reconstituted specimens of Merville clay

Test	w(%) before creep	Consolidation stress (kPa)		Applied stress for creep Δq (kPa)	OCR
		First stage p'_{max}	Second stage p'_0		
CRE1 / OCR=2	36.2	700	350 (350#)	350 (344#)	2.0#
CRE2 / OCR=3.5	37.0	700	200 (203#)	200 (198#)	3.4#
CRE3 / OCR=7	40.9	700	100 (102#)	100 (100#)	6.9#
CRE4 / OCR=14	41.0	700	50 (52#)	50 (52#)	13.5#
CRE5 / OCR=2*	36.3	700	350 (350#)	350 (349#)	2.0#

Remarks: CRE representing creep test, # for real measured value during tests.

Figure captions

Fig. 1 Results of undrained triaxial tests on specimens with OCR=1 in compression, with OCRs from 1 to 14 in compression, and with OCRs of 1 and 4 in extension respectively: (a,c,e) deviatoric stress and normalized stress (q/p'_{max}) versus axial strain for tests of (b,d,f) stress path in the plane of p'-q and p'/p'_{max} -q/p'_{max}

Fig. 2 Results of undrained triaxial tests on specimens with different OCRs in compression and in extension with isotropic compression stages plotted in e-logp'

Fig. 3 Results of undrained triaxial cyclic tests on specimens with OCR=4 under different cyclic stress ratio R_c from 0.22 to 0.52: (a, d, g, j) deviatoric stress versus mean effective stress, (b, e, h, k) deviatoric stress versus axial strain, and (c, f, i, l) excess pore pressure versus axial strain

Fig. 4 Axial strain versus the number of cycles under different cyclic stress ratio for (a) R_c = 0.22, (b) R_c = 0.44, (c) R_c = 0.48, (d) R_c = 0.52

Fig. 5 Results of undrained triaxial cyclic tests on specimens with OCR=4 under different cyclic stress ratio R_c from 0.22 to 0.52: (a) permanent axial strains versus the number of cycles, and (b) cyclic axial strains versus the number of cycles

Fig. 6 Excess pore pressure versus the number of cycles under different cyclic stress ratio for (a) R_c = 0.22, (b) R_c = 0.44, (c) R_c = 0.48, (d) R_c = 0.52

Fig. 7 Results of undrained triaxial cyclic tests on specimens with OCR=4 under different cyclic stress ratio R_c from 0.22 to 0.52: (a) permanent excess pore pressure versus the number of cycles, and (b) cyclic excess pore pressure versus the number of cycles

Fig. 8 Results of undrained triaxial creep tests: (a) axial strain versus time, (b) excess pore pressure versus time, (c) enlarged initial early parts of the curves of axial strain versus time shown in Fig. 8(a), and (d) enlarged initial early parts of the curves of excess pore pressure versus time shown in Fig. 8(b)

Fig. 9 Relationship between stress ratio (q/p') and elapsed time of creep

Fig. 10 Stress path in p'-q plane for undrained triaxial creep tests: (a) from the beginning of loading to maximum stress ratio (q/p') and (b) from maximum stress ratio (q/p') to the end of creep test

Fig. 11 Evolution of undrained creep test results in *e*-log(*p*') plane: (a) test time from the beginning of loading to 1 minute, (b) test time at 10th minute, (c) test time at 100th minute, and (d) from maximum stress ratio (*q*/*p*') to the end of creep test

Fig. 12 Results of undrained triaxial creep tests: (a) plastic deviatoric strain rate versus elapsed time of creep, (b) plastic volumetric strain rate versus elapsed time of creep, and (c) enlarged the final parts of the relationship between plastic volumetric strain rate and elapsed time of creep shown in Fig. 12(a)

Fig. 13 Evolutions of dilatancy *d* versus stress ratio during undrained creep stages

Fig. 14 Comparisons of excess pore pressures versus number of cycles or time between undrained triaxial cyclic tests under different cyclic stress ratios and undrained triaxial creep tests under different over-consolidation ratios

Figure 1

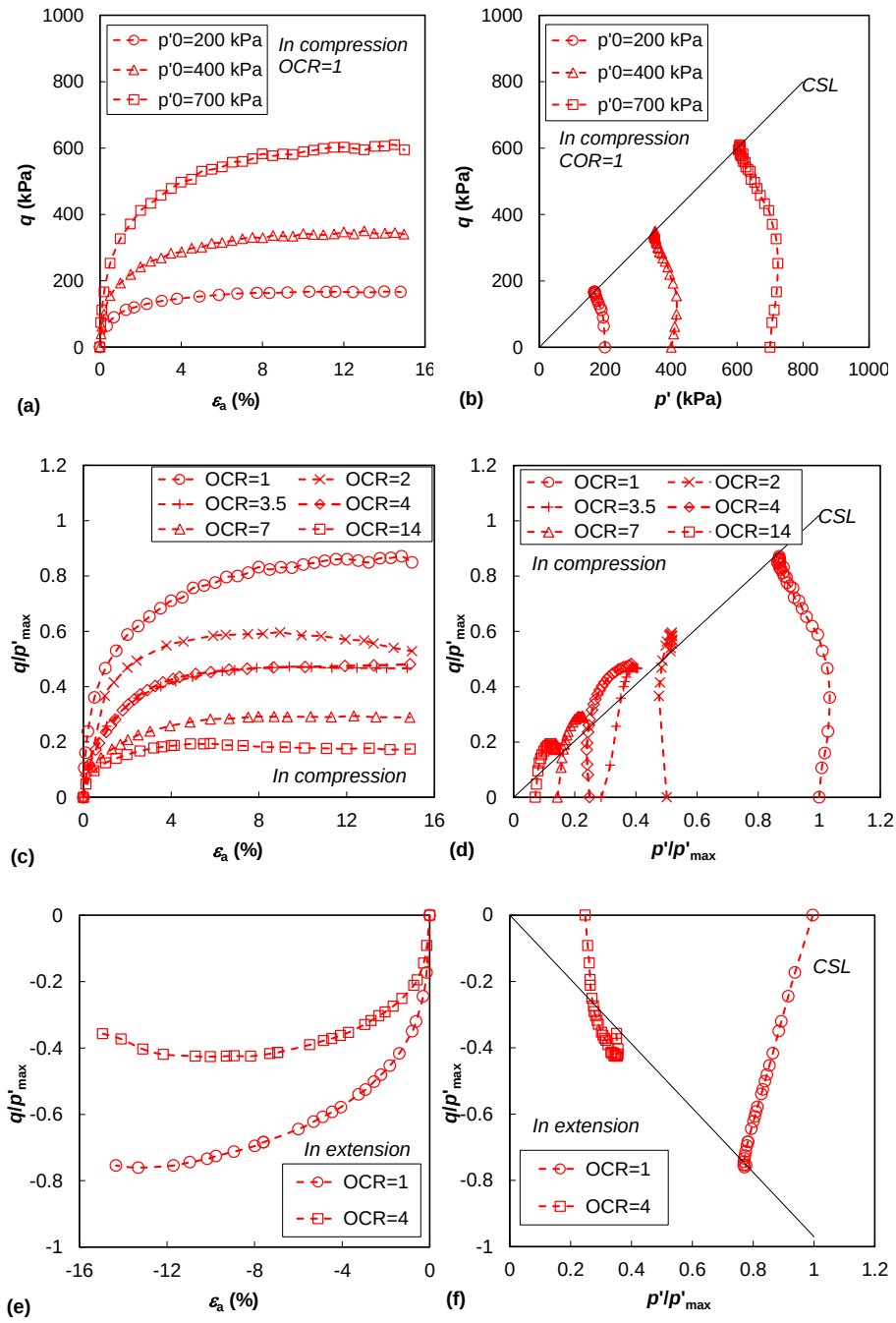
p'0=200 kPa
p'0=400 kPa
p'0=700 kPa
In compression
OCR=1
q (kPa)
εa (%)
(a)
CSL
In compression
COR=1
p' (kPa)
(b)
OCR=1
OCR=2
OCR=3.5
OCR=4
OCR=7
OCR=14
q/p'max
In compression
(c)
p'/p'max
(d)
In extension
(e)
(f)

Figure 2

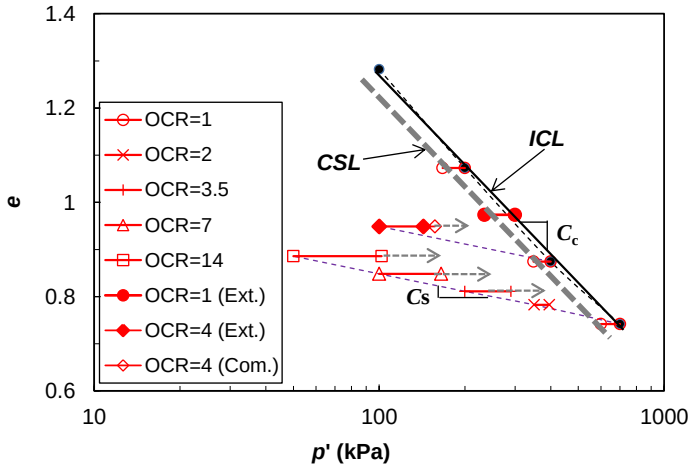
1.4
1.2
1
0.8
0.6
e
10
100
1000
p' (kPa)
OCR=1
OCR=2
OCR=3.5
OCR=7
OCR=14
OCR=1 (Ext.)
OCR=4 (Ext.)
OCR=4 (Com.)
CSL
ICL
Cc
Cs

Figure 3

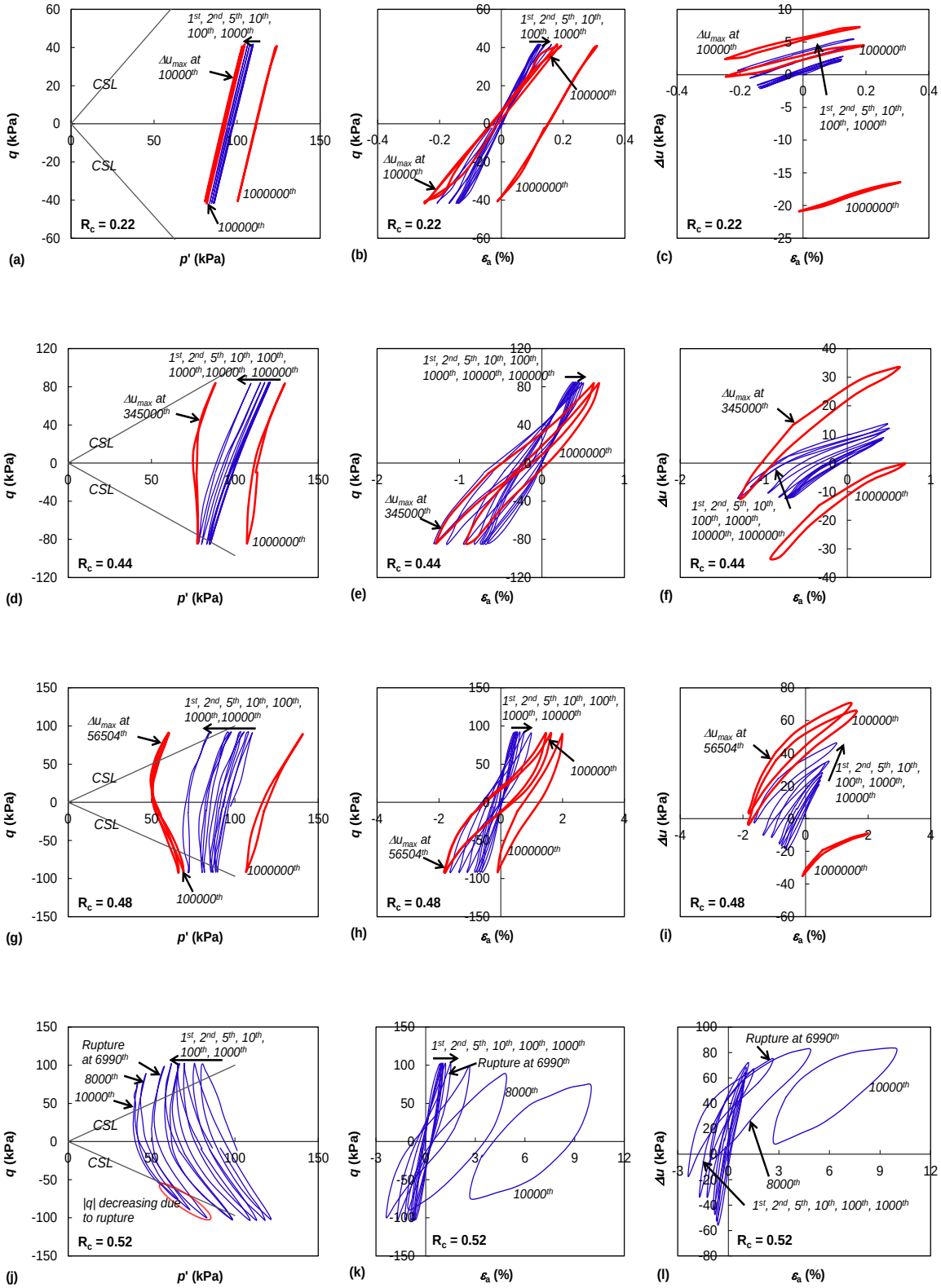
(a)
(b)
(c)
(d)
(e)
(f)
(g)
(h)
(i)
(j)
(k)
(l)
q (kPa)
p' (kPa)
εa (%)
Δu (kPa)
CSL
Δumax at 10000th
Δumax at 345000th
Δumax at 56504th
1st, 2nd, 5th, 10th, 100th, 1000th
1st, 2nd, 5th, 10th, 100th, 1000th,10000th
1st, 2nd, 5th, 10th, 100th, 1000th, 10000th, 100000th
1000000th
100000th
10000th
8000th
Rupture at 6990th
Rupture at 6990th
|q| decreasing due to rupture
Rc = 0.22
Rc = 0.44
Rc = 0.48
Rc = 0.52

Figure 4

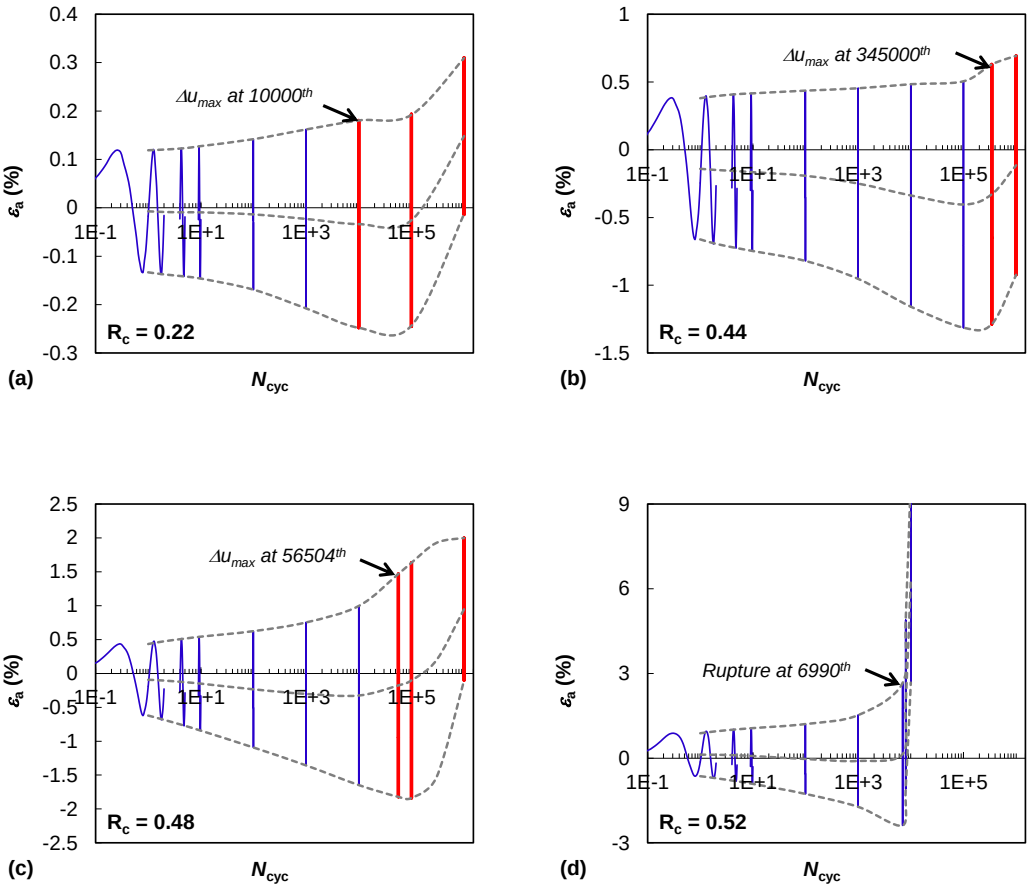
0.4
0.3
0.2
0.1
0
-0.1
-0.2
-0.3
Δu_max at 10000th
ε_a (%)
1E-1
1E+1
1E+3
1E+5
R_c = 0.22
(a)
N_cyc
1
0.5
0
-0.5
-1
-1.5
Δu_max at 345000th
R_c = 0.44
(b)
2.5
2
1.5
1
0.5
0
-0.5
-1
-1.5
-2
-2.5
Δu_max at 56504th
R_c = 0.48
(c)
9
6
3
0
-3
Rupture at 6990th
R_c = 0.52
(d)

Figure 5

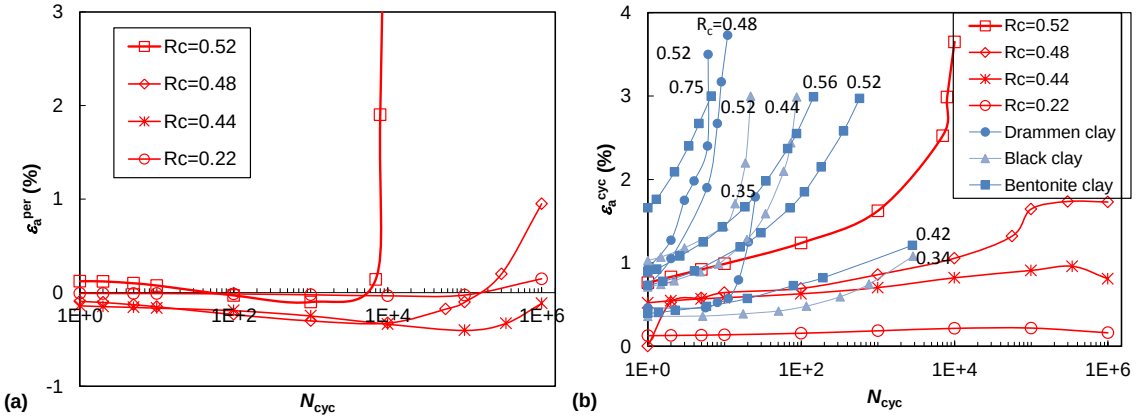
Rc=0.52
Rc=0.48
Rc=0.44
Rc=0.22
ε_a^{per} (%)
N_{cyc}
(a)
R_c=0.48
0.52
0.75
0.52
0.44
0.56
0.52
0.35
0.42
0.34
Drammen clay
Black clay
Bentonite clay
ε_a^{cyc} (%)
N_{cyc}
(b)

Figure 6

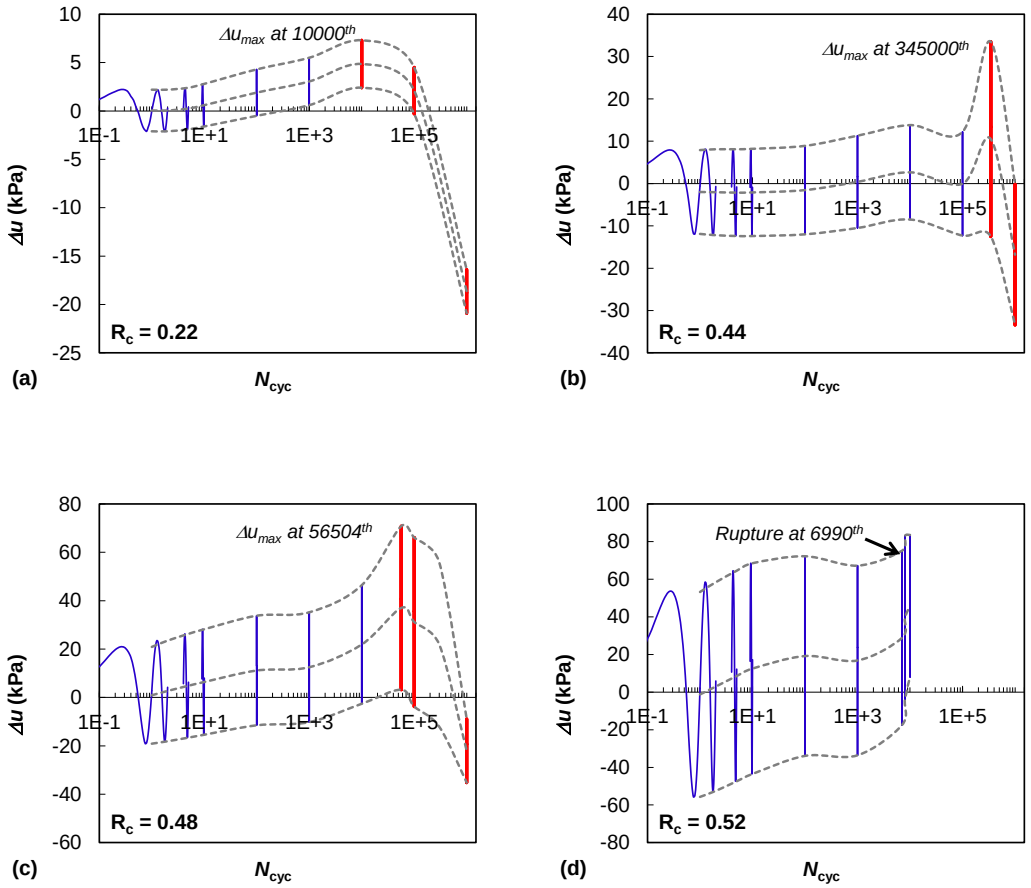
Δu_max at 10000th
R_c = 0.22
(a)
Δu_max at 345000th
R_c = 0.44
(b)
Δu_max at 56504th
R_c = 0.48
(c)
Rupture at 6990th
R_c = 0.52
(d)
Δu (kPa)
N_cyc
1E-1
1E+1
1E+3
1E+5

Figure 7

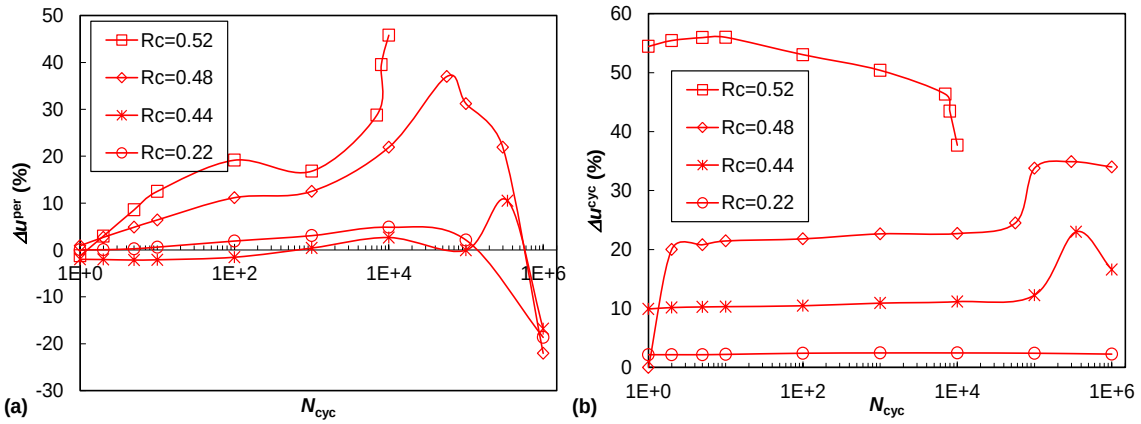

Figure 8

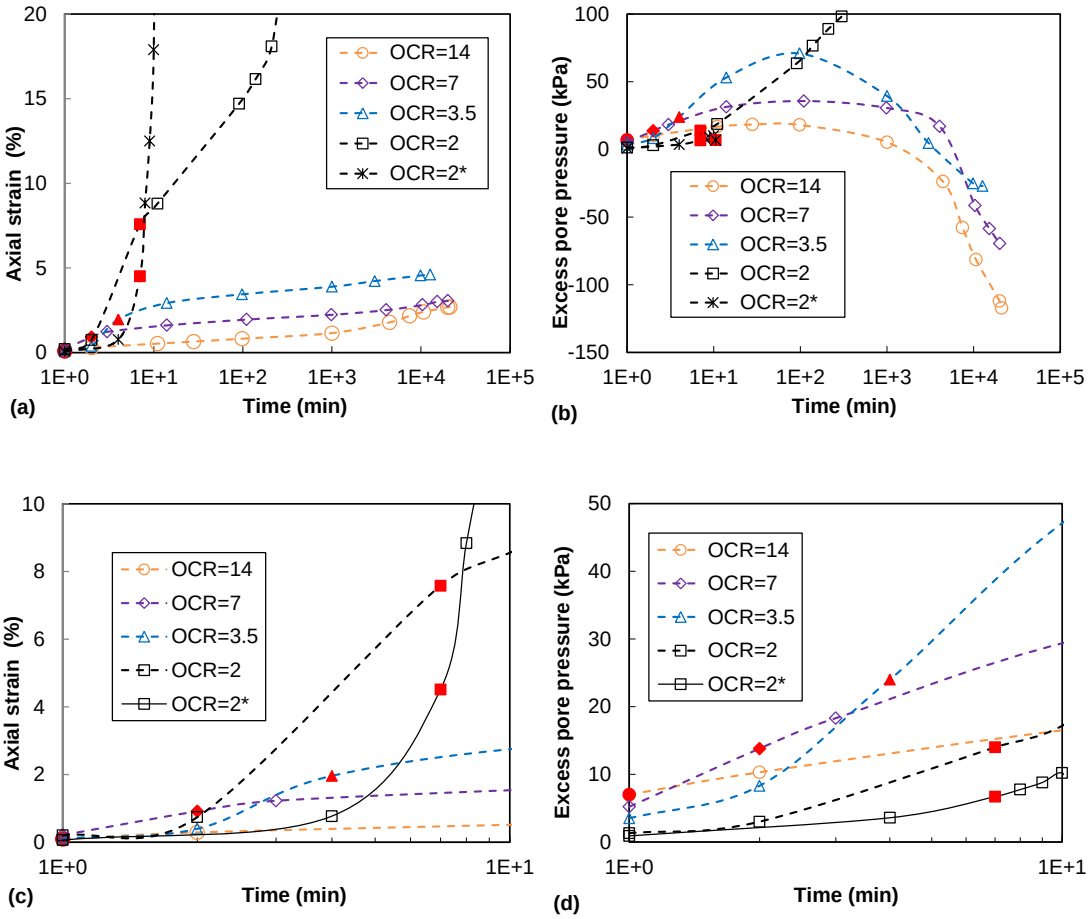
Axial strain (%)
Time (min)
(a)
OCR=14
OCR=7
OCR=3.5
OCR=2
OCR=2*
Excess pore pressure (kPa)
Time (min)
(b)
Axial strain (%)
Time (min)
(c)
Excess pore pressure (kPa)
Time (min)
(d)

Figure 9

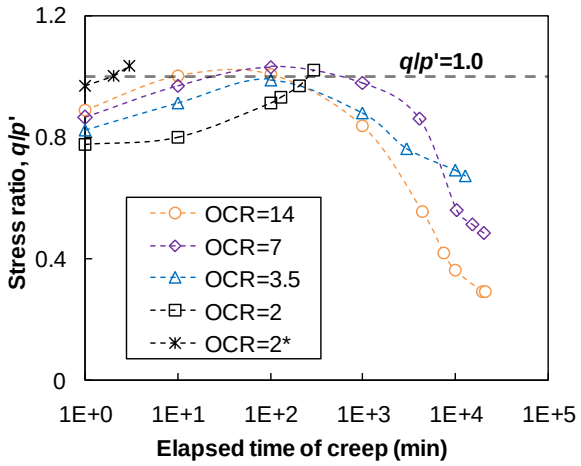
1.2
0.8
0.4
0
Stress ratio, q/p'
q/p'=1.0
OCR=14
OCR=7
OCR=3.5
OCR=2
OCR=2*
1E+0
1E+1
1E+2
1E+3
1E+4
1E+5
Elapsed time of creep (min)

Figure 10

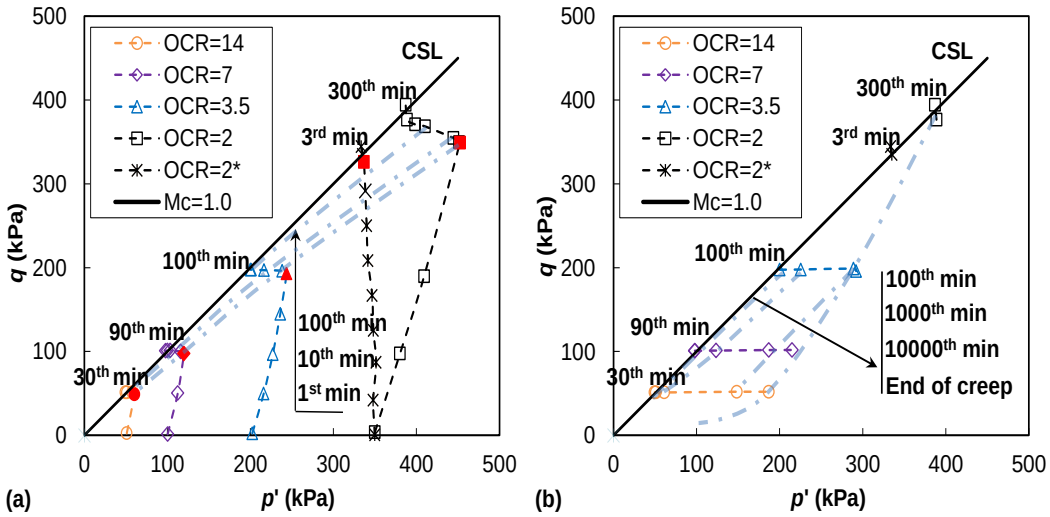
OCR=14
OCR=7
OCR=3.5
OCR=2
OCR=2*
Mc=1.0
CSL
300th min
3rd min
100th min
90th min
30th min
100th min
10th min
1st min
q (kPa)
p' (kPa)
(a)
100th min
1000th min
10000th min
End of creep
(b)

Figure 11

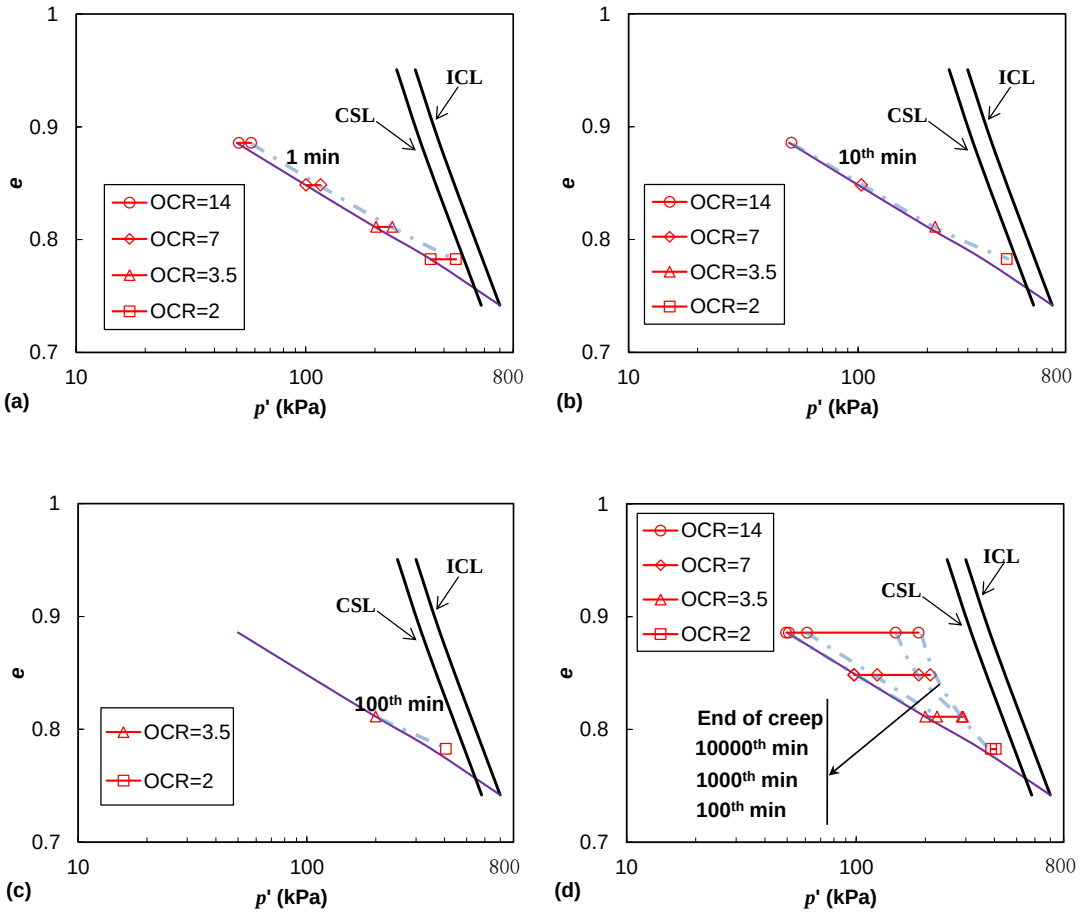
1
0.9
0.8
0.7
e
10
100
800
p' (kPa)
ICL
CSL
1 min
OCR=14
OCR=7
OCR=3.5
OCR=2
(a)
10th min
(b)
100th min
(c)
End of creep
10000th min
1000th min
100th min
(d)

Figure 12

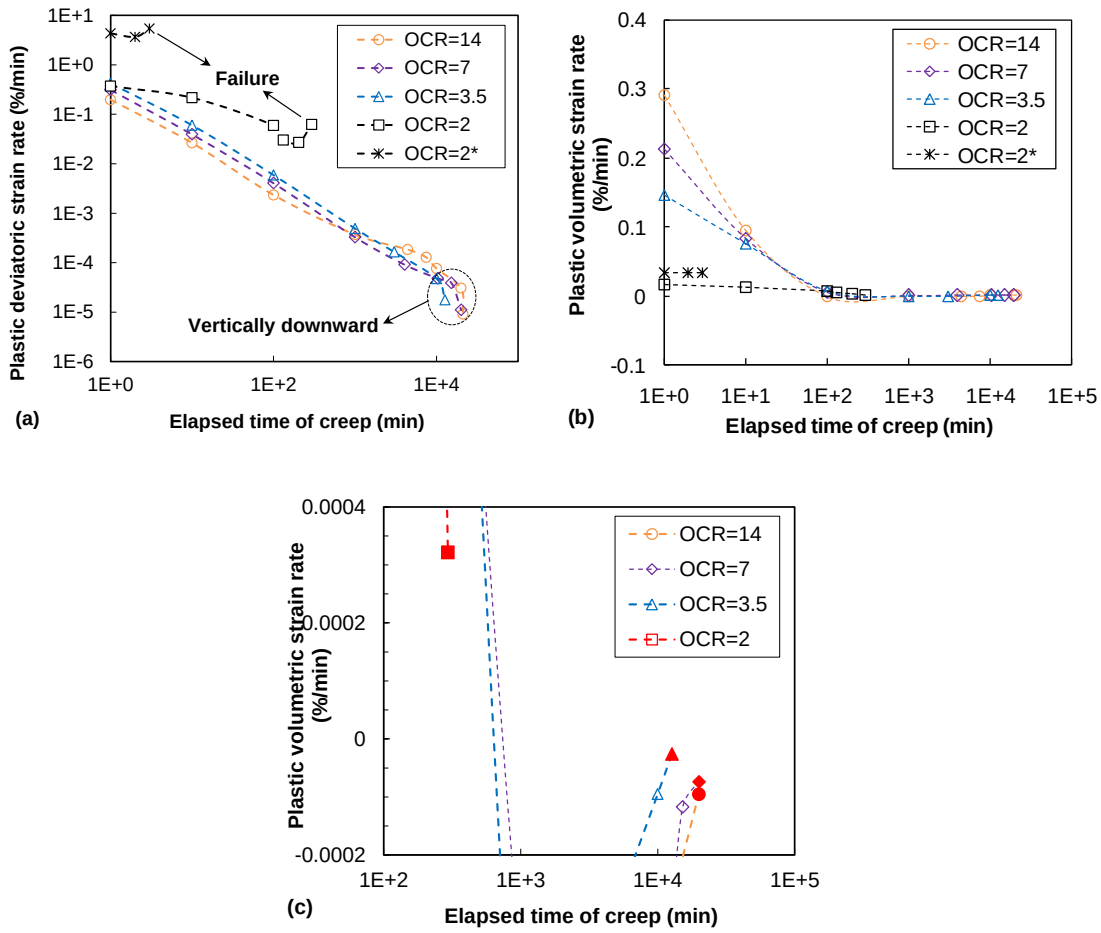
Plastic deviatoric strain rate (%/min)
1E+1
1E+0
1E-1
1E-2
1E-3
1E-4
1E-5
1E-6
1E+0
1E+2
1E+4
Elapsed time of creep (min)
(a)
Failure
Vertically downward
OCR=14
OCR=7
OCR=3.5
OCR=2
OCR=2*
Plastic volumetric strain rate (%/min)
0.4
0.3
0.2
0.1
0
-0.1
1E+0
1E+1
1E+2
1E+3
1E+4
1E+5
Elapsed time of creep (min)
(b)
OCR=14
OCR=7
OCR=3.5
OCR=2
OCR=2*
Plastic volumetric strain rate (%/min)
0.0004
0.0002
0
-0.0002
1E+2
1E+3
1E+4
1E+5
Elapsed time of creep (min)
(c)
OCR=14
OCR=7
OCR=3.5
OCR=2

Figure 13

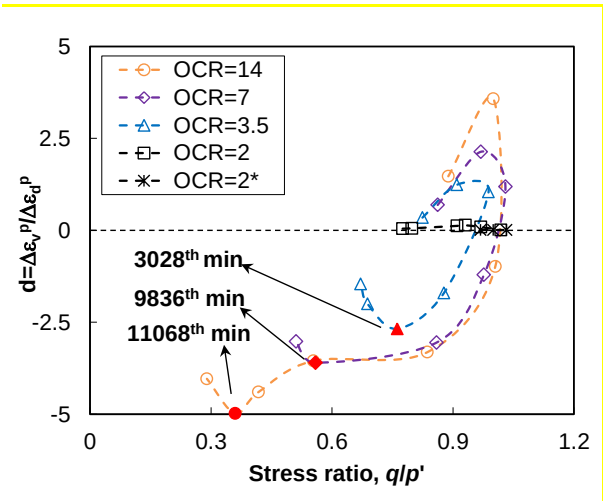
OCR=14
OCR=7
OCR=3.5
OCR=2
OCR=2*
3028th min
9836th min
11068th min
d=Δεv p/Δεd p
Stress ratio, q/p'
5
2.5
0
-2.5
-5
0
0.3
0.6
0.9
1.2

Figure 14

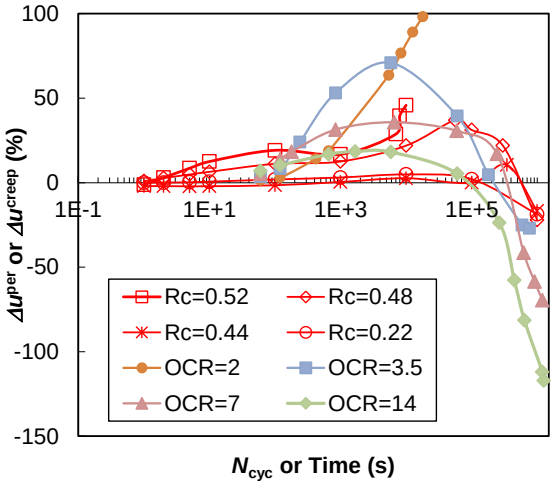
100
50
0
-50
-100
-150
1E-1
1E+1
1E+3
1E+5
Δu^per or Δu^creep (%)
N_cyc or Time (s)
Rc=0.52
Rc=0.48
Rc=0.44
Rc=0.22
OCR=2
OCR=3.5
OCR=7
OCR=14